VOL. 11, NO. 1, JANUARY 2016 ISSN 1819-6608
ARPN Journal of Engineering and Applied Sciences

www.arpnjournals.com

EFFECT OF GEOMETRICAL PARAMETERS ON BOILING HEAT TRANSFER AND PRESSURE DROP IN MICRO FINNED MICRO GAP

Shugata Ahmed[1], Muhammad Hasibul Hasan[2], Ahmad Faris Ismail[1] and Erwin Sulaeman[1]
[1]Departmental of Mechanical Engineering, Faculty of Engineering, Jalan Gombak, Kuala Lumpur, Malaysia
[2]Departmental of Manufacturing and Materials Engineering, Faculty of Engineering, Jalan Gombak, Kuala Lumpur, Malaysia
shugataahmed@gmail.com

ABSTRACT

Micro gap heat sinks are potential candidates of evaporative cooling. Additional fins in micro gap enhance heat transfer rate by increasing surface area and generating turbulence. The scope of this paper is to numerically investigate the influence of various geometrical parameters on thermal and hydraulic performance of a micro finned micro gap during flow boiling. For this purpose, flow boiling of water in a micro finned micro gap heat sink has been simulated using FLUENT 14.5 release. Thermal resistance and pressure drop have been calculated for various fin width-to-fin spacing ratio and ratio of base thickness-to-micro gap height. The results demonstrate that thermal resistance decreases for increasing both ratios. However, the descending rate is inconsistent. For higher ratios, decrement rate of thermal resistance is very slow, while pressure drop is very high. Hence, it is suggested that the dimensions should be optimized for extensive cooling performance.

Keywords: micro fin, micro gap, flow boiling, thermal resistance, pressure drop.

INTRODUCTION

Thermal management of electronic devices is one of the important aspects of electronic packaging specially for developing microelectromechanical systems (MEMS) or advanced very large-scale integrated (VLSI) circuits. With these rapid advancing technologies, it is necessary to develop new methodologies to remove higher heat fluxes from the component surface to avoid any possible damage. Microchannels are considered as a solution of thermal management system of ingrowing power dissipation from digital devices with high gate density. It has high heat dissipation capability resulting from its large heat transfer surface-to-volume ratio. This advantageous characteristic of microchannels was noted first by Tuckerman and Peace [1]. They found that dissipated heat flux from a 60 µm wide and 302 µm deep channel is up to790 Wm^{-2}, while using water as an energy transmission fluid. However, the pressure drop was more than 2 bars and stream wise surface temperature rise was also very high as thermal boundary layer develops in the flow direction. Due to higher pressure drop, higher pumping power is required to drive the fluid through microchannels.

Besides of high pumping power requirement, microchannel heat sinks show temperature and pressure instabilities during flow boiling. Micro gap heat sinks can effectively reduce flow boiling instabilities [2].

Alam *et al*. [3] investigated heat transfer and pressure drop characteristics of three different micro gaps of190 µm, 285 µm and 381 µm heights. Experimental results showed that heat transfer coefficient increases with the decrement of gap size. On the other hand, pressure drop is higher for smaller gap sizes. However, in another publication, Alam *et al*. [4] stated that below100 µm, dry out takes place very early. Hence, it is not suitable for cooling purpose. They showed that the gap size should be between $100 - 500$ µm for effective cooling.

Micro fins can be effectively used with micro gap heat sinks for high performance cooling. In Figure-1, a micro finned micro gap heat sink created by ANSYS Workbench Design Modeler has been shown. Fin shapes, dimensions and fin spacing play key role in heat transfer and pressure drop characteristics of micro finned structures. Optimization of these parameters can enhance heat transfer rate. Some of the key findings in this area are stated below from literature.

Cooling efficiency of micro fins of different cross-sectional shapes has been investigated numerically by Abdoli *et al*. [5]. They highly recommended convex lens shape micro fins over circular and hydrofoil designs as there is a significant reduction of surface temperature and pumping power. Adewumi *et al*. [6] optimized microchannels with micro fins. Thermal conductance was the objective function to be maximized by optimizing hydraulic diameter, aspect ratio, solid volume fraction and aspect ratio of micro pin fins. Micro pin finned minichannels were also investigated and optimized by Tullius *et al*. [7]. They used six different shapes of micro fins among which triangular fins showed best thermal performance. They optimized height, width and fin spacing to maximize the heat transfer rate. The heat transfer phenomenon of heat sinks with micro pin fins has been explored experimentally by Liu *et al*. [8]. They showed that micro finned heat sinks possess high heat transfer capability. According to them, thermal resistance of the heat sink decreases with increasing pressure drop. Shafeie *et al*. [9] also studied the effect of micro pin fins

on microchannels. Their results showed that micro pin finned structures perform slightly better than optimized conventional microchannel heat sink for small pumping power. Flow boiling in a micro finned structure is also found highly efficient for cooling, although pressure drop penalty is higher than smooth surfaces.

This paper concerns with the effect of various dimensions on two-phase heat transfer and pressure drop of pure water in micro finned micro gap. Flow boiling of water in this particular heat sink of 30 mm × 30 mm footprint area has been simulated using FLUENT 14.5 release. Thermal resistance and pressure drop have been plotted for various fin width-to-fin spacing ratio and base thickness-to-gap height ratio.

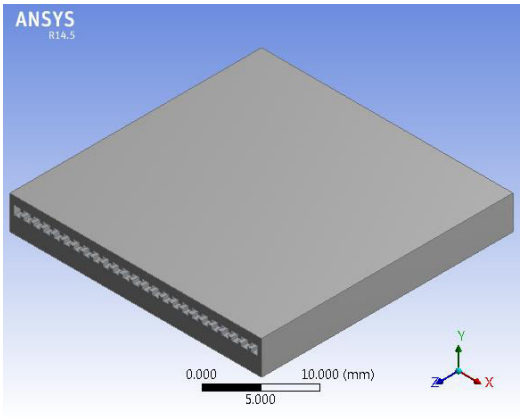

Figure-1. Micro finned micro gap (3D view)

MATHEMATICAL MODEL

Governing equations

Volume of Fluid (VOF) model [10] has been used for flow modelling. From Eqn. (1) – (4) are steady-state governing equations for flow boiling and heat transfer, which have been solved further by applying proper boundary conditions. Details of CFD analysis has been followed from publication of Kelvin *et al*. [11]

The void fraction equation is given below:

$$\rho_v \nabla(\alpha . \vec{v}_v) = \dot{m}_{l\to v} - \dot{m}_{v\to l} \quad (1)$$

Here ρ_v and $\vec{v}_v$ are density and velocity of vapor respectively. $\dot{m}_{l\to v}$ and $\dot{m}_{v\to l}$ represent mass transfer from liquid to vapor and vice versa respectively.

For a Newtonian fluid, conservation of momentum equation is the following:

$$\rho\nabla(\vec{v}.\vec{v}) = -\nabla P + \nabla\tau + \rho\vec{g} + \vec{F}_\sigma \quad (2)$$

In Equation (2), ∇P and $\nabla\tau$ are pressure and shear stress gradients respectively, $\vec{g}$ is the gravitational acceleration and $\vec{F}_\sigma$ denotes the surface tension force.

Conservation of energy equation for fluid domain is written as:

$$\rho_v \nabla(\alpha . E_v . \vec{v}_v) = \nabla\left(k_{eff}\nabla\theta_v\right) + h_{lv}(\dot{m}_{v\to l} - \dot{m}_{l\to v}) \quad (3)$$

Here E_v and θ_v are enthalpy and temperature of vapor respectively, k_{eff} represents effective thermal conductivity and h_{lv} is the enthalpy of vaporization.

For solid domain, the energy equation can be written as:

$$\nabla(k_s\nabla\theta) = 0 \quad (4)$$

Here $C_{p,s}$ and θ are specific heat capacity and temperature of the solid domain respectively.

Mass exchange between two phases is calculated from evaporation-condensation model, proposed by Lee [12].

$$\dot{m}_{l\to v} = \varepsilon * (1-\alpha)\rho_l \frac{(T_l - T_{sat})}{T_{sat}} \quad (5)$$

$$\dot{m}_{v\to l} = \upsilon * \alpha\rho_v \frac{(T_{sat} - T_v)}{T_{sat}} \quad (6)$$

Here, ε and υ are evaporation and condensation coefficients, respectively. Wu *et al*. [13], De Schepper et al. [14] and Alizadehdakhel *et al*. [15] recommended the value 0.1 of these coefficients to maintain interfacial temperature close to saturation temperature, T_{sat}.

Governing equations for turbulence have been derived from Renormalization Group Theory (RNG) based k − ε turbulence model [16], which are given below:

$$\rho\nabla(\vec{v}.k) = \nabla\left(a_k.\mu_{eff}.\nabla k\right) + G_k + G_b - \rho\varepsilon - Y_M + S_k \quad (7)$$

$$\rho\nabla(\vec{v}.\varepsilon) = \nabla\left(a_\varepsilon.\mu_{eff}.\nabla\varepsilon\right) + C_{1\varepsilon}\frac{\varepsilon}{k}(G_k + C_{3\varepsilon}G_b) - C_{2\varepsilon}\rho\frac{\varepsilon^2}{k} - R_\varepsilon + S_\varepsilon \quad (8)$$

In above equations, k and ε are turbulent kinetic energy and rate of energy dissipation respectively.

G_k = generation of turbulent kinetic energy due to the mean velocity gradients

G_b = generation of turbulent kinetic energy due to buoyancy

Y_M = contribution of the fluctuating dilatation in compressible turbulence to the overall dissipation rate

a_k and a_ε are inverse effective Prandtl numbers for k and ε respectively and S_k and S_ε are source terms.

The model constants have following default values:

$C_{1\varepsilon}$ = 1.42, $C_{2\varepsilon}$ = 1.68

Following dimensional ratios have been considered:

$$\beta = \frac{W_f}{d} \quad (9)$$

$$\gamma = \frac{h_g}{\delta} \quad (10)$$

In above equations, W_f is fin width, d is the distance between two fins, h_g is the gap height and δ is the lower base thickness.

Total thermal resistance is the summation of conductive and convective thermal resistance, which is obtained from following equation:

$$R_{th} = R_{cond} + R_{conv} = \frac{H}{k_s A_s} + \frac{1}{hA_f} \quad (11)$$

A_s and A_f represent available area of heat transfer in solid and fluid respectively.

Boundary conditions

Following boundary conditions are applied in the computational domain:

Inlet: $T_f = T_{in}$, $\dot{m} = \dot{m}_{in}$, $\alpha = 0$. In this study, inlet temperature of water has been kept constant at 25℃.

Outlet: $P = P_{out}$. Atmospheric pressure is defined at the outlet of the heat sink.

Solid-fluid interface: Heat transfer from wall to fluid by convection, $q_{eff} = h(\theta - \theta_f)$.

Channel bottom wall: Uniform heat flux is applied at the bottom of the heat sink. Heat is transferred through solid wall by conduction in the normal direction of bottom surface, $q = -k_s \frac{\partial \theta}{\partial n}$.

Other channel walls: Other channel walls are considered as insulated. Hence, $\frac{\partial \theta}{\partial n} = 0$.

GEOMETRY, MESHING AND NUMERICAL SOLUTION

The geometry has been generated by ANSYS Workbench Design Modeler. Dimensional ranges of the sink are provided in Table-1. Heat sink material is aluminium. After creating geometry, fine meshing has been done. Number of meshing elements has been optimized to reduce computational time. Fluid flow and heat transfer are considered steady-state.

FLUENT uses Finite Volume Method to solve governing equations. Second Order Upwind scheme has been used for spatial discretization of the governing equations. Semi-Implicit Method for Pressure Linked Equations (SIMPLE) algorithm, developed by Patankar and Spalding [17] has been adopted to solve pressure-velocity coupling equation.

Table-1. Dimensions of heat sink, micro gap and fins.

Parameters (unit)	**Value**
Heat sink height, H (mm)	4
Heat sink width, W (mm)	30
Heat sink length, L (mm)	30
Fin width-to-fin spacing ratio (β)	0.2-2.174
Base thickness-to-gap height ratio (γ)	0.2-2
Number of fins, **N**	48

RESULTS AND DISCUSSIONS

Heat transfer

In Figure-2, thermal resistance of the heat sink has been plotted for various fin width-to-fin spacing ratios(β), while base thickness-to-gap height ratio (γ) has been kept conntant at 2. Applied heat flux is $10^7 \mathrm{Wm}^{-2}$ and mass flow rate is$0.059\ \mathrm{kgs}^{-1}$. For this particular mass flow rate, Reynolds number is higher than 2400. Hence, it is estimated that the flow is turbulent. From figure, it is observed that thermal resistance decreases with increasing β, although decrement rate is low for higher ratios. When fin width increases, fin spacing decreases. As a result, β increases. Due to the increament of fin width, available area for conduction (A_s) increases. Hence, conductive thermal resistance R_{cond} decreases. On the other hand, area for convection (A_f) decreases with the decrement of fin spacing. At first, the descending nature of conductive thermal resistance dominates the total thermal resistance (R_{th}) of the heat sink. As a result, R_{th} decreases steeply. However, for higher ratios, dominance of R_{cond} is reduced by increment ofR_{conv}. Hence, decrement rate of R_{th} becomes slow. A similar phenomenon was also observed by Hung *et al.* [18] for nano-fluid cooled double-layer microcahnnel heat sink.

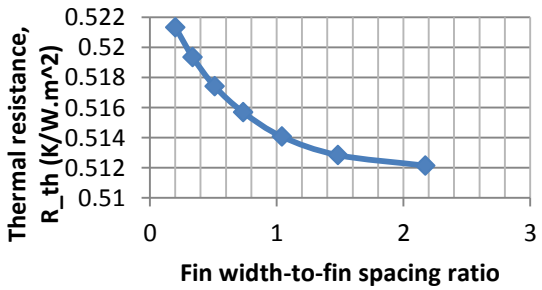

Figure-2. Thermal resistance vs. fin width-to-fin spacing ratio for $10^7 \mathrm{Wm}^{-2}$ heat flux and $0.059\ \mathrm{kgs}^{-1}$ mass flow rate.

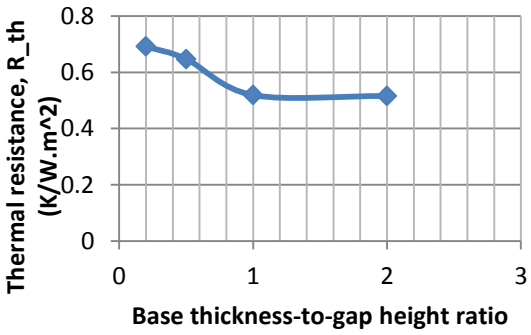

Figure-3. Thermal resistance vs. base thickness-to-micro gap height ratio for $10^7 \mathrm{Wm}^{-2}$ heat flux and 0.059 kgs^{-1} mass flow rate.

In Figure-3, R_{th} has been plotted for various base thickness-to-micro gap height ratios (γ), while $\beta = 0.7353$. It shows that R_{th} decreases up to $\gamma = 1$. After that, thermal resistance does not change with further increment of γ. γ increases due to the increment of base thickness (δ) as well as decrement of gap height (h_g). According to Alam et al. [3], heat transfer coefficient (h) increases with the decrement of gap size. As a result, R_{th} decreases. However, after $\gamma = 1$, effect of dimensions on h decreases. As a result, change of R_{th} is found negligible. Area-weighted average heat transfer coefficient is plotted for various γ in Figure-4.

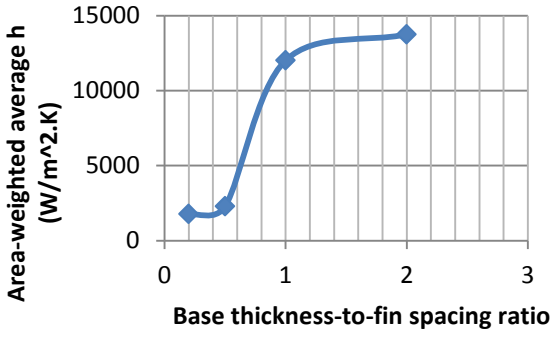

Figure-4. Area-weighted average heat transfer coefficient vs. base thickness-to-micro gap height ratio for $10^7 \mathrm{Wm}^{-2}$ heat flux and 0.059 kgs^{-1} mass flow rate.

Pressure drop

Contour plot of pressure drop in the micro gap for $\beta = 2.1739$ and $\gamma = 2$ has been shown in Figure-5. It is seen that pressure decreases in the flow direction.

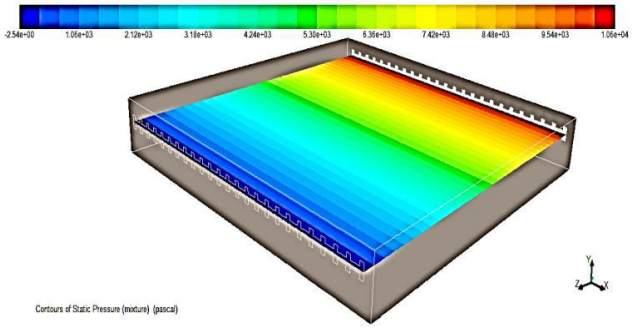

Figure-5. Contour plot of pressure distribution on X-Z plan at Y=2.5 mm for $\beta = 2.1739$ and $\gamma = 2$.

In Figure-6, pressure drop has been plotted for variousβ. It is found that pressure drop increases linearly with the increment ofβ. As cross-sectional area of the channel decreases with increasingβ, pressure drop increases.

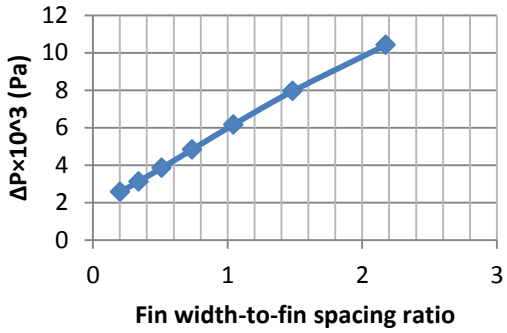

Figure-6. Pressure drop vs. base thickness-to-micro gap height ratio for $10^7 \mathrm{Wm}^{-2}$ heat flux and 0.059 kgs^{-1} mass flow rate.

Increment of pressure drop with the increment of γ is observed in Figure-7. Micro gap height decreases with the increment of γ. Hence, pressure drop rises. Alam et al. [3] also stated that pressure drop is high for smaller gap sizes. However, it is found that the increment rate is high from $\gamma = 0.5$ to 1 and decreases slightly from $\gamma = 1$ to 2.

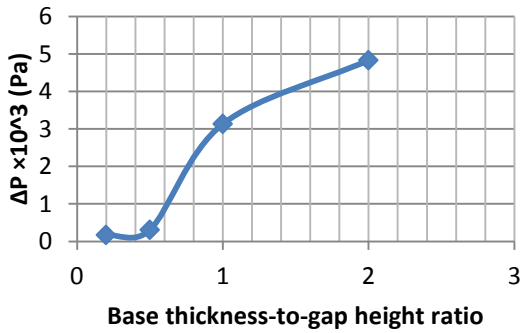

Figure-7. Pressure drop vs. base thickness-to-micro gap height ratio for $10^7 \mathrm{Wm}^{-2}$ heat flux and and 0.059 kgs^{-1} mass flow rate.

CONCLUSIONS

Thermal and hydraulic characteristics of a micro finned micro gap for different dimensions of fin and heat sink have been studied. From the results, it has been found that thermal resistance decreases with the increment of fin width-to-fin spacing ratio and base thickness-to-gap height ratio. However, decrement rate is high for lower ratios. When dimensional ratios increases, decrement rate of thermal resistance slows down. Moreover, pressure drop is high for higher dimensional ratios. As higher pressure drop requires high pumping power, it can be estimated that lower dimensional ratios are better for both effective cooling and low cost. However, proper optimization may increase the cooling efficiency of the heat sink.

A limitation of the current study is that a steady-state solver has been used for simulation, which does not take temperature and pressure drop fluctuations with time in account. Hence, it is expected that a transient solver may provide better results.

ACKNOWLEDGEMENT

The support of the Ministry of Education, Malaysia under the grant FRGS 14-131-0372 is gratefully acknowledged. This research was also supported by International Islamic University Malaysia from Endowment Type B fund (EDW B14-127-1012).

REFERENCES

[1] Tuckerman B. and Pease R. F. W. 1981. High-performance heat sinking for VLSI. Electron Device Letters, IEEE 2.5. pp. 126 –129.

[2] Alam T., Lee P. S., Yap C. R. and Jin L. W. 2011. Experimental investigation of microgap cooling technology for minimizing temperature gradient and mitigating hotspots in electronic devices. 13th Electronics Packaging Technology Conference (EPTC). pp. 530-535.

[3] Alam T., Lee P. S., Yap C. R. and Jin L. W. 2012. Experimental investigation of local flow boiling heat transfer and pressure drop characteristics in microgap channel. International Journal of Multiphase Flow. 42: 164-174.

[4] Alam T., Lee P. S., Yap C. R., Jin L. W. and Balasubramanian K. 2012. Experimental investigation and flow visualization to determine the optimum dimension range of microgap heat sinks. International Journal of Heat and Mass Transfer. 55(25): 7623-7634.

[5] Abdoli A., Jimenez G. and Dulikravich G. S. 2015. Thermo-fluid analysis of micro pin-fin array cooling configurations for high heat fluxes with a hot spot. International Journal of Thermal Sciences. 90: 290-297.

[6] Adewumi O. O., Bello-Ochende T. and Meyer J. P. 2013. Constructal design of combined microchannel and micro pin fins for electronic cooling. International Journal of Heat and Mass Transfer. 66: 315-323.

[7] Tullius J. F., Tullius T. K. and Bayazitoglu Y. 2012. Optimization of short micro pin fins in minichannels. International Journal of Heat and Mass Transfer. 55(15): 3921-3932.

[8] Liu M., Liu D., Xu S. and Chen Y. 2011. Experimental study on liquid flow and heat transfer in micro square pin fin heat sink. International Journal of Heat and Mass Transfer. 54(25): 5602-5611.

[9] Shafeie H., Abouali O., Jafarpur K. and Ahmadi G. 2013. Numerical study of heat transfer performance of single-phase heat sinks with micro pin-fin structures. Applied Thermal Engineering. 58(1): 68-76.

[10] Hirt C. W. and Nichols B. D. 1981. Volume of fluid (VOF) method for the dynamics of free boundaries. Journal of Computational Physics. 39(1): 201-225.

[11] Kelvin H.C.S., Yousif A.A. and Andrew C. 2012. Unsteady heat transfer in an annular pipe, Part II: swirling laminar flow. IIUM Engineering Journal. 12(6): 79-95.

[12] Lee W. H. 1979. A Pressure Iteration Scheme for Two-Phase Modeling, Technical Report LA-UR. Los Alamos Scientific Laboratory, Los Alamos, New Mexico. pp. 79-975.

[13] Wu H. L., Peng X. F., Ye P. and Gong Y. E. 2007. Simulation of Refrigerant Flow Boiling in Serpentine Tubes. International Journal of Heat and Mass Transfer. 50(5): 1186–1195.

[14] De Schepper, S. C., Heynderickx G. J. and Marin G. B. 2009. Modeling the Evaporation of a Hydrocarbon Feedstock in the Convection Section of a Steam Cracker. Computers and Chemical Engineering. 33(1): 122–132.

[15] Alizadehdakhel A., Rahimi M. and Alsairafi A. A. 2010. CFD Modeling of Flow and Heat Transfer in a Thermosyphon. International Communications in Heat and Mass Transfer. 37(3): 312-318.

[16] Orszag S. A., Yakhot V., Flannery W. S., Boysan F., Choudhury D., Maruzewski J. and Patel B. 1993. Renormalization Group Modeling and Turbulence Simulations. International Conference on Near-Wall Turbulent Flows, Tempe, Arizona. pp. 1031-1046.

[17] Patankar S. V. and Spalding, D. B. 1972. A calculation procedure for heat, mass and momentum transfer in three-dimensional parabolic flows. International Journal of Heat and Mass Transfer. 15(10): 1787-1806.

[18] Hung T. C. and Yan W. M. 2012. Enhancement of thermal performance in double-layered microchannel heat sink with nanofluids. International Journal of Heat and Mass Transfer. 55(11): 3225-3238.